Research Square

Preprints are preliminary reports that have not undergone peer review.
They should not be considered conclusive, used to inform clinical practice,
or referenced by the media as validated information.

Quantizing photosynthetic performance of phytoplankton using photosynthesis-irradiance response models

Xiaolong Yang
Fudan University https://orcid.org/0000-0002-9763-6122
Lihua Liu
Jinggangshan University
Zhikai Yin
Fudan University Department of Environmental Science and Engineering
Xingyu Wang
Fudan University Department of Environmental Science and Engineering
Shoubing Wang (bswang@fudan.edu.cn)
https://orcid.org/0000-0003-2696-2083
Zipiao Ye
Jinggangshan University

Research

Keywords: Phytoplankton, Photosynthetic performance, irradiance, photosynthesis-irradiance response model

Posted Date: December 20th, 2019

DOI: https://doi.org/10.21203/rs.2.19403/v1

License: This work is licensed under a Creative Commons Attribution 4.0 International License.
Read Full License

Version of Record: A version of this preprint was published at Environmental Sciences Europe on February 26th, 2020. See the published version at https://doi.org/10.1186/s12302-020-00306-9.

Quantizing photosynthetic performance of phytoplankton using photosynthesis-irradiance response models

Xiaolong Yang [a], Lihua Liu [b], Zhikai Yin [a], Xingyu Wang [a], Shoubing Wang [a,*], Zipiao Ye [b,*]

[a] Department of Environmental Science and Engineering, Fudan University, 2005 Songhu road, Shanghai 200433, PR China

[b] Institute of Biophysics, Maths & Physics College, Jinggangshan University, 28 Xueyuan road, Ji'an 343009, PR China

* Corresponding author: Prof. Shoubing Wang

Fax: +86-21-65642297, E-mail: bswang@fudan.edu.cn

Corresponding author: Prof. Zipiao Ye

Fax: +86-796-8100488, E-mail: yezp@jgsu.edu.cn

Abstract

Background: Clarifying the relationship between photosynthesis and irradiance and accurately quantizing photosynthetic performance are of importance to calculate the productivity of phytoplankton, whether in aquatic ecosystems modelling or obtaining more economical production.

Results: The photosynthetic performance of seven phytoplankton species was

characterized by four typical photosynthesis-irradiance (*P-I*) response models. However, the differences were found between the returned values to photosynthetic characteristics by different *P-I* models. The saturation irradiance (I_{sat}) was distinctly underestimated by model 1, and the maximum net photosynthetic rate (P_{nmax}) was quite distinct from its measured values, due to the asymptotic function of the model. Models 2 and 3 lost some foundation to photosynthetic mechanisms, that the returned I_{sat} showed significant differences with the measured data. Model 4 for higher plants could reproduce the irradiance response trends of photosynthesis well for all phytoplankton species and obtained close values to the measured data, but the fitting curves exhibited some slight deviations under the low intensity of irradiance. Different phytoplankton species showed differences in photosynthetic productivity and characteristics. *P. subcordiformis* showed larger intrinsic quantum yield (α) and lower I_{sat} and light compensation point (I_c) than *D. salina* or *I. galbana*. *Microcystis* sp., especially *M. aeruginosa* with the largest P_{nmax} and α among freshwater phytoplankton strains, exhibited more efficient light use efficiency than two species of green algae.

Conclusions: The present work will be useful both to describe the behavior of different phytoplankton in a quantitative way as well as to evaluate the flexibility and reusability of *P-I* models. Meanwhile we believe this research could provide important insight into the structure changes of phytoplankton communities in the aquatic ecosystems.

Keywords: Phytoplankton; Photosynthetic performance; irradiance; photosynthesis-irradiance response model

Background

Phytoplankton are a key functional component of aquatic ecosystems, play a pivotal role in biogeochemical cycles [1]. In particular, marine phytoplankton, as the principal driving force of ocean carbon cycles and energy flows, fix approximately 50 gigatons of inorganic carbon annually, almost half of the total global primary production [2, 3]. They show higher CO_2 fixation rates and higher biomass productivity than any other photosynthetic organism [3]. With increasing concentration of CO_2 concentrations in the atmosphere and growing climate warming, an accurate estimate of photosynthetic productivity of phytoplankton becomes ever more important for modelling primary production and structure changes of phytoplankton communities in aquatic ecosystems, especially eutrophic lakes (e.g., Taihu, Erie, Winnipeg lake) and estuaries (e.g., Yangtze River).

Clarifying the relationship between photosynthesis and irradiance is a basis to evaluate the growth performance of phytoplankton. Irradiance acts as a driving force in photosynthesis. The level of irradiance affects the growth, CO_2 fixation efficiency, carbon metabolism, and cell composition of photosynthetic organisms [4-8]. While extensive studies have been carried out and many insights have enriched the basis of phytoplankton physiology in recent decades [9-11], the relationship remains poorly understood for phytoplankton. High irradiance causes photoinhibition by the production of reactive oxygen species (ROS) and damages the function of the most light-sensitive complex PSII [5]. Irradiance availability affects phytoplankton community composition and is one of the key factors causing cyanobacteria blooms [12]. Resource competition theory shows that species with lower “critical light intensity” are often superior, such as *Microcystis* [13].

On the other hand, phytoplankton cells are rich in proteins, polysaccharides, lipids, vitamins, and polyunsaturated fatty acids, which have stirred up great attention as a promising potential feedstock for biofuel, nutraceuticals, animal and aquaculture feed production [10, 14]. Many species have been used for commercial development, such as *Dunaliella salina*, *Isochrysis galbana*, *Spirulina* (or *Arthrospira*), *Haematococcus pluvialis*, and *Scenedesmus obliquus* [2, 6, 10]. Almost all fishes, bivalve molluscs, and crustaceans primarily graze on phytoplankton to build immunity against diseases during their early larval stages [12]. However, large-scale production of phytoplankton has rarely been successful, with no more than 1 g DW L^{-1} biomass that is mainly limited by the inefficiency of photosynthesis in high-cell density cultivation [11, 14, 15]. The photosynthetic parameters can be seen as indicators to achieve sustainable carbon assimilation and TAG accumulation in *Isochrysis zhangjiangensis* [8]. Therefore, accurately quantizing photosynthetic performance is crucial for more economical integration of production management and operation of industrial-scale phytoplankton culture systems [16].

The response curve of photosynthesis to irradiance (*P-I*) is frequently used to characterize photosynthetic performance by fitting experimental data (measured as oxygen evolution or carbon uptake) with *P-I* models [17]. Obtained photosynthetic parameters, including the maximum net photosynthetic rate (P_{nmax}), the optimal intensity of irradiance (I_{sat}), and the dark respiration rate (R_d) can be regarded as indicator to evaluate the response of phytoplankton to meet environmental changes. A variety of *P-I* models for phytoplankton have been established in the last few decades [18-30]. Although many recent models are suggested based to “old models” established in the 70s and 80s and have some contributions to improve, the most extensive application are still found in

those “old models” [31-35]. For example, an examination of the literature overwhelmingly reveals in excess of 1950 papers on the model proposed by Platt et al.[20]. This is most probably because they are simpler than those new models with complex parameters and any new model must take many years to be fully adopted. Higher plant and phytoplankton possess similar photosynthetic systems. Ye et al. developed a model for higher plants that parameterizes the core characteristics of the irradiance response, including solar energy absorption of photosynthetic pigment molecules, energy transfer, and electron transport between photosynthetic apparatuses[36]. This has been widely applied in rice, wheat, soybean, sunflower and other plants [37, 38].

The objective of this study was to determine the various relationships between the photosynthetic productivity of phytoplankton and irradiance intensity and investigate the reliability of *P-I* models to estimate the photosynthetic performance for phytoplankton. We selected the rather extensive range of phytoplankton, including three isolated from the ocean and four from lakes, to measure their photosynthetic oxygen evolution under different irradiance intensity. Obtained *P-I* data were fitted by using *P-I* model for quantization the photosynthetic performances. One *P-I* model for higher plants developed by Ye et al.[36] (it was represented as model 4 in this study) was first used to compare against three most widely applied models for phytoplankton (them were represented as models 1, 2 and 3 in this study).

Materials and methods

Phytoplankton cultivation

The three strains of marine phytoplankton (*Isochrysis galbana*, *Dunaliella salina* and *Platymonus subcordiformis*) isolated from East China Seas were grown aseptically in f/2 medium. The four strains of freshwater phytoplankton (*Microcystis aeruginosa* FACHB-

905, *Microcystis wesenbergii* FACHB-1112, *Scenedesmus obliquus* FACHB-116 and *Chlorococcum* sp. FACHB-1556) were purchased from the Freshwater Algae Culture Collection (FACHB-collection) of the Institute of Hydrobiology, Chinese Academy of Sciences (Wuhan, China) and cultivated in BG11 medium. The cultures were illuminated by cool white fluorescent bulbs (60 μmol photons m^{-2} s^{-1}) with a photoperiod of 12 h per day at 26 ± 1 °C.

Measurement of photosynthetic oxygen evolution

After seven to ten days of incubation, the photosynthetic oxygen-evolving rate of microalgal cells reaching the exponential growth phase was determined using a bio-oxygen metre (Yaxin-1151, Beijing Yaxinliyi Science and Technology Co., Ltd., China). Eight-mL cell suspensions of each strain were exposed to increasing orders of irradiance intensity (0, 25, 50, 100, 150, 200, 300, 400, 500, 600, 800, 1000, and 1200 μmol photons m^{-2} s^{-1}), given by a digital LED light source (YX-11LA, Beijing Yaxinliyi Science and Technology Co., Ltd., China), at 25 ± 1 °C. The metre took reads once every three seconds for 5 min in each irradiance measurement point, during which a linear relationship varying with time in oxygen concentration was obtained. Triplicate samples were prepared and measured for each test. The response of the photosynthetic oxygen-evolving rate to irradiance was fitted with four *P-I* models [18-20, 22, 36].

Determination of chlorophyll a concentration and cell counts

The cells for photosynthetic oxygen-evolving measurement were collected by centrifugation (5600 × g) for 10 min at 4 °C. Chlorophyll *a* (Chl *a*) was extracted from microalgal cells in 90% (v/v) acetone and left overnight at 4 °C in darkness. The extracts were then centrifuged at 3600 × g for 10 min. The Chl *a* concentration was determined spectrophotometrically in the supernatant with a SP752 UV-vis spectrophotometer

(Spectrum Instruments, Shanghai, China) according to the method of Jeffrey & Humphrey [39]. One-mL cultures of each strain were taken and preserved in Lugol's iodine solution for counting algal cells by a haemocytometer. Each test was conducted in triplicate.

Model description

Model 1

The light dependence of the net photosynthetic rate (P_n) is expressed as [22]:

$$P_n = P_{nmax}\tanh\left(\frac{\alpha I}{P_{nmax}}\right) - R_d \quad (1)$$

where P_n (μmol O_2 mg^{-1} Chl *a* h^{-1}) is the chlorophyll *a*-normalised net photosynthetic rate at irradiance I, P_{nmax} (μmol O_2 mg^{-1} Chl *a* h^{-1}) is the light-saturated maximum rate of photosynthesis, α (μmol O_2 mg^{-1} Chl *a* h^{-1} / μmol photons m^{-2} s^{-1}) is the light-limited initial slope, and R_d (μmol O_2 mg^{-1} Chl *a* h^{-1}) is the dark respiration rate.

The saturation irradiance (I_{sat}, μmol photons m^{-2} s^{-1}) corresponding to the light-saturated maximum rate (P_{nmax}) of photosynthesis is calculated as [1]:

$$I_{sat} = \frac{P_{nmax} - R_d}{\alpha} \quad (2)$$

But the analytic solution of the light compensation point (I_c, μmol photons m^{-2} s^{-1}) can not be obtained by equation (1). In order to obtain I_c, Kok effect [40] must be ignored here, and I_c can be calculated as [19]:

$$I_c = \frac{R_d}{\alpha} \quad (3)$$

The photosynthetic quantum efficiency (P_n', μmol O_2 μmol photons $^{-1}$) is calculated as:

$$P_n' = \frac{\alpha}{cosh^2\frac{\alpha I}{P_{nmax}}} \quad (4)$$

Model 2

The light dependence of P_n is expressed as [19, 20]:

$$P_{\mathrm{n}} = P_{\mathrm{s}}\left[1-exp\left(-\frac{\alpha I}{P_{\mathrm{s}}}\right)\right]exp\left(-\frac{\beta I}{P_{\mathrm{s}}}\right) - R_{\mathrm{d}} \quad (5)$$

where P_{n} is the chlorophyll *a*-normalised net photosynthetic rate at irradiance I; P_{s} is the parameter reflecting the maximum, potential, light-saturated, rate of photosynthesis; α is the light-limited initial slope; β is the dimensionless parameter reflecting the photoinhibition process; and R_{d} is the dark respiration rate.

The I_{sat} is calculated as:

$$I_{\mathrm{sat}} = \frac{P_{\mathrm{s}}}{\alpha} ln \frac{\alpha+\beta}{\beta} \quad (6)$$

The P_{nmax} can be calculated as:

$$P_{\mathrm{nmax}} = P_{\mathrm{s}}\left(\frac{\alpha}{\alpha+\beta}\right)\left(\frac{\beta}{\alpha+\beta}\right)^{\frac{\beta}{\alpha}} - R_{\mathrm{d}} \quad (7)$$

However, the analytic solution of I_{c} can not be obtained by equation (5). To obtain I_{c}, the Kok effect must be ignored here, and I_{c} can be calculated as:

$$I_{\mathrm{c}} = \frac{R_{\mathrm{d}}}{\alpha} \quad (8)$$

The photosynthetic quantum efficiency is calculated as:

$$P'_{\mathrm{n}} = exp\left(-\frac{\beta I}{P_{\mathrm{s}}}\right)\left\{\alpha\, exp\left(-\frac{\alpha I}{P_{\mathrm{s}}}\right) - \beta\left[1 - exp\left(-\frac{\alpha I}{P_{\mathrm{s}}}\right)\right]\right\} \quad (9)$$

Model 3

The light dependence of P_{n} is expressed as [18]:

$$P_{\mathrm{n}} = \frac{I}{\alpha I^2+\beta I+\gamma} - R_{\mathrm{d}} \quad (10)$$

Here P_{n} is the chlorophyll *a*-normalised net photosynthetic rate at irradiance I; α and β are the fundamental parameters, nondimensional; and R_{d} is the dark respiration rate. The reciprocal of γ is the light-limited initial slope.

I_{sat} is calculated as:

$$I_{\text{sat}} = \sqrt{\frac{\gamma}{\alpha}} \tag{11}$$

P_{nmax} is given by:

$$P_{\text{nmax}} = \frac{1}{\beta+2\sqrt{\alpha\gamma}} - R_d \tag{12}$$

When $P_{\text{n}} = 0$, I_{c} is given as follows,

$$I_{\text{c}} = \frac{1-\beta R_d+\sqrt{(1-\beta R_d)^2-4\alpha\gamma R_d}}{2\alpha R_d} \tag{13}$$

The photosynthetic quantum efficiency is calculated as:

$$P'_{\text{n}} = \frac{\gamma-\alpha I^2}{(\gamma+\beta I+\alpha I^2)^2} \tag{14}$$

Model 4

The light dependence of P_{n} is expressed as [36]:

$$P_{\text{n}} = \alpha\frac{1-\beta I}{1+\gamma I} I - R_{\text{d}} \tag{15}$$

Here P_{n} is the chlorophyll *a*-normalised net photosynthetic rate at irradiance I, α is the initial slope of the P_{n}-I response curve, β and γ are the nondimensional parameters reflecting photoinhibition and light saturation, respectively, and R_{d} is the dark respiration rate.

I_{sat} is calculated as:

$$I_{\text{sat}} = \frac{\sqrt{\frac{(\beta+\gamma)}{\beta}}-1}{\gamma} \tag{16}$$

P_{nmax} is obtained by:

$$P_{\text{nmax}} = \alpha\left(\frac{\sqrt{\beta+\gamma}-\sqrt{\beta}}{\gamma}\right)^2 - R_d \tag{17}$$

When $P_{\text{n}} = 0$, I_{c} is given as follows,

$$I_{\text{c}} = \frac{\alpha-\gamma R_d-\sqrt{(\alpha-\gamma R_d)^2-4\alpha\beta R_d}}{2\alpha\beta} \tag{18}$$

The photosynthetic quantum efficiency is calculated as:

$$P_{\mathrm{n}}^{'} = \alpha \frac{1-2\beta I-\beta\gamma I^2}{(1+\gamma I)^2} \quad (19)$$

Statistical analysis

P-I data were fitted using SPSS version 24.0 using nonlinear, least-squares fitting based on the Levenberg–Marquardt algorithm. Duncan's post hoc tests ($p < 0.05$) were performed to establish differences among fitted results from model 1, model 2, model 3 and model 4. Data were reported as the means and standard errors in the calculations. Goodness of fit of the mathematical models to experimental data was assessed using the adjusted coefficient of determination (R^2).

Results

Comparison of different *P-I* models of production curves

Applying different values of the fundamental parameters to the model, the differences in the characteristics of production curves among model 2, model 3 and model 4 were compared, save for model 1, without consideration of light-inhibition at high irradiant intensity. Assuming that the initial slope α was 0.5 (the initial slope of the curve equals the reciprocal of γ in model 3), increasing values of the light-saturated or photoinhibition parameters decreased P_{nmax} of the curve and increased the magnitude of inhibition in three types (Fig. 1b-f), which indicated that they could closely reproduce the trend of the P_{n}-I curve. However, although P_{s} is defined as being associated with P_{nmax} in model 2, the given value of P_{s} was over 30 ~ 125% of P_{nmax}, for which the biological implication is difficult to understand (Fig. 1a). However, in Fig. 1c, I_{sat} was kept constant value versus the change of β because I_{sat} was barely related to α or γ, according to Eqn. 16. In fact, greater β values were associated with greater bends of the curve, indicating saturation occurred more easily. Thus, Fig. 1c is clearly contradictory to the basis of photosynthetic

physiology.

The morphological and growth characteristics of phytoplankter

The morphology of the cultured cells was observed under a 600x optical microscope. Cells were mostly spherical, at 4.3 ~ 10 μm in diameter, and grew singly, except for *S. obliquus*. The Chl *a* contents were 1.647 ± 0.015, 2.778 ± 0.077, 2.297 ± 0.027, 1.320 ± 0.005, 1.739 ± 0.012, 1.318 ± 0.027 and 4.158 ± 0.077 mg L^{-1} for cultures of *I. galbana*, *D. salina*, *P. subcordiformis*, *M. aeruginosa*, *M. wesenbergii*, *S. obliquus* and *Chlorococcum* sp., respectively (Table 1), which was used to normalize the photosynthetic oxygen-producing rate of phytoplankton. This normalization will reduce the variability of photosynthetic oxygen-producing rates as a result of differences in biomass, facilitating the comparison of photosynthetic performance. The Chl *a* content per cell of *I. galbana*, *D. salina*, *P. subcordiformis*, *M. aeruginosa*, *M. wesenbergii*, *S. obliquus*, and *Chlorococcum* sp. was 2.570 ± 0.042, 27.118 ± 1.151, 22.931 ± 0.563, 1.972 ± 0.044, 2.404 ± 0.031, 9.126 ± 0.600, and 4.578 ± 0.106 ng 10^4 $cells^{-1}$, respectively.

***P-I* curve and *P′-I* curve of freshwater phytoplankton**

The *P-I* curves for *M. aeruginosa*, *M. wesenbergii*, *S. obliquus* and *Chlorococcum* sp. are given in Fig. 3A. For almost all strains, P_n increased rapidly with *I* under low irradiance intensity, and reached saturation at 400 μmol photons m^{-2} s^{-1}. P_n exhibited a sharp decline for *M. aeruginosa*, *M. wesenbergii*, and *S. obliquus* yet only a slow decline for *Chlorococcum* sp. with the increasing *I*. As was observed for marine phytoplankton, all curves exhibited photoinhibition above the I_{sat}, but in addition to those estimated by model 1.

M. aeruginosa and *M. wesenbergii* are two different species of *Microcystis* sp., and

despite having nearly identical *P-I* curves, there were some differences in the photosynthetic parameters obtained by the different models (Table 3). The values of P_{nmax} obtained by models 2, 3 and 4 were close to their measured values (approximately 290.83 μmol O_2 mg^{-1} Chl *a* h^{-1} for *M. aeruginosa* and 201.29 μmol O_2 mg^{-1} Cha h^{-1} for *M. wesenbergii*), with < 5% of errors. Nevertheless, the values of I_{sat} calculated by models 2 and 3 for *M. aeruginosa* and *M. wesenbergii* were far below their measured values, with significant differences ($p < 0.05$). For *S. obliquus*, the values of P_{nmax} obtained by models 2, 3 and 4 were just under 1% of the measured value, yet all the corresponding I_{sat} were over the measured value. The P_{nmax} calculated by models 2, 3 and 4 for *Chlorococcum* sp. were 75.25 ± 3.79, 76.15 ± 3.89 and 74.59 ± 4.23 μmol O_2 mg^{-1} Chl *a* h^{-1}, respectively, while the I_{sat} were 311.04 ± 17.27, 339.85 ± 15.19 and 396.06 ± 15.9 μmol photons m^{-2} s^{-1}, respectively. No significant differences were found between the I_{sat} calculated by model 4 and the measured data ($p < 0.05$). The photosynthetic parameters obtained by model 1 were still far from the measured data for these freshwater phytoplankton; above all, the I_{sat} were seriously underestimated. For α, the estimated by model 4 was the highest for all strains among the other three models. There were no significant differences in the estimation of I_c or R_d among each model. Fig. 3B indicates that the nonlinear change of P'_n as I in four species of freshwater phytoplankton was similar to that in marine phytoplankton.

_P-I_ curve and _P′-I_ curve of marine phytoplankton

The *P-I* curves of *I. galbana*, *D. salina* and *P. subcordiformis* are shown in Fig. 2A, and obvious differences were observed among strains. P_n increased gradually with I towards saturation, which was at 800 μmol photons m^{-2} s^{-1} for *I. galbana*. However, for *D. salina* and *P. subcordiformis*, P_n increased steeply, almost linearly, within low

281 irradiance intensity (below 200 μmol photons m^{-2} s^{-1}), and it decreased rapidly when it
282 reached the maximum value. All curves stopped above the I_{sat}, excluding those produced
283 by model 1, which indicates the presence of photoinhibition.

284 Differences were also observed in photosynthetic characteristic parameters calculated
285 by the four types of models (Table 2). Model 1 either overestimated P_{nmax} or
286 underestimated I_{sat}, and these values showed significant differences with their measured
287 values ($p < 0.05$) for three strains of marine phytoplankton. The P_{nmax} obtained by models
288 2, 3 and 4 for *I. galbana* were 97.45 ± 3.02, 97.55 ± 3.37 and 98.33 ± 3.20 μmol O_2 mg^{-1}
289 Chl *a* h^{-1}, respectively. The I_{sat} corresponding to P_{nmax} were 709.60 ± 26.89, 699.26 ±
290 32.19, 766.17 ± 24.38 μmol photons m^{-2} s^{-1}, respectively. Despite no significant
291 differences in either estimated P_{nmax} or I_{sat} by the three models ($p > 0.05$), model 4 fitted
292 the values to the measured values with < 5% of errors. For *D. salina*, the P_{nmax} estimated
293 by models 2, 3 and 4 were 113.73 ± 6.24, 114.45 ± 6.24 and 113.31 ± 5.87 μmol O_2 mg^{-1}
294 Chl *a* h^{-1}, respectively, while the I_{sat} obtained by model 2 and model 3 were notably lower
295 than the measured value, with significant differences ($p < 0.05$). The I_{sat} obtained by
296 model 4 was 510.24 ± 2.92 μmol photons m^{-2} s^{-1}, which was quite similar to the measured
297 value (approximately 500 μmol photons m^{-2} s^{-1}). The values of P_{nmax} estimated by models
298 2, 3 and 4 for *P. subcordiformis* were 94.64 ± 6.65, 95.59 ± 6.63, and 92.20 ± 6.56 μmol
299 O_2 mg^{-1} Chl *a* h^{-1}, respectively; however, the calculated I_{sat} were significantly higher than
300 the measured values ($p < 0.05$), likely because of the rapid increase of P_n during low-
301 intensity irradiance. The initial slope of the *P-I* curve α, namely, the intrinsic quantum
302 yield, estimated by model 4 was higher for all strains than those estimated by other models,
303 with significant differences ($p < 0.05$) for *D. salina* and *P. subcordiformis*.

304 The photosynthetic quantum yield represents the efficiency of carbon dioxide fixation

or oxygen evolution by a photosynthetic apparatus driven by absorbed photon energy, that is, the conversion efficiency of absorbed solar energy into chemical energy. Fig. 2B shows that the quantum yield calculated by models 2, 3 and 4 for *I. galbana*, *D. salina* and *P. subcordiformis* decreased as I increased, until it was equal to zero at the I_{sat} point. Subsequently, it became negative as I increased, which also reveals why P_n decreased as I increased above I_{sat}. However, the values of P'_n obtained by model 1 were always greater than zero with increasing I due to the asymptotic function in this model.

Discussion

Photosynthesis is not only a biochemical process achieved by photosynthetic apparatuses, it also contains a biophysical process [5, 9, 41]. As shown in Fig. 4, photosynthetic pigment molecules (*Chl*), such as Chlorophyll *a* and *b* and carotenoids, absorb solar energy, which induces them into an excited state (*Chl**). The largest amount of exciton binding energy is transferred to the photochemical reaction centres (P_{680} and P_{700}), where charge separation occurs and produces electrons (e^-) and accompanied by the splitting of water into P_{680}*. Other energy is transformed into fluorescence and heat [5, 17, 25, 28, 29]. *Chl** conducts de-excitation by photochemistry, non-radiation heat dissipation, and chlorophyll fluorescence then able to accept new photons, yet the process depend on the lifetime of *Chl* in the excited state [41, 42]. The released electrons pass through pheophytin to the first electron acceptor Q_A and are ultimately transferred via a series of electron carriers to photosystem I, thereby producing ATP and reducing NADPH to driving photosynthetic carbon fixation and respiratory carbon oxidation [5, 26]. Although a variety of *P-I* models have been established and used to fit the *P-I* curve for estimating photosynthetic performance and responses to environment changes for phytoplankton [18-20, 22-30, 43], many of them were not built based on the

photosynthetic mechanism.

The exponential model established by Webb et al. [23] and model 1 are still applied extensively for phytoplankton [31-35] even though they lack photoinhibition function. For example, Ma et al. [34] indicated that the P_{nmax} calculated by model 1 for *M. aeruginosa* FACHB-905 and *M. aeruginosa* FACHB-469 were 253.92 ± 6.79 and 231.32 ± 6.40 μmol O_2 mg^{-1} Chl *a* h^{-1}, respectively, at 25 °C, yet the corresponding I_{sat} were only 92.71 ± 7.86 and 88.61 ± 3.22 μmol photons m^{-2} s^{-1}, respectively. Furthermore, the shape of their *P-I* curves did not appear to decline above I_{sat}. In our study, the values of α, P_{nmax} and I_{sat} fitted by model 1 showed significant differences with those obtained by other models ($p < 0.05$); either P_{nmax} or I_{sat} were distinct from their measured data for seven strains of phytoplankton (including *M. aeruginosa* FACHB-905), which suggests that an insufficient irradiance would be supplied to the cultivation if the I_{sat} was used as the optimal intensity of irradiance.

To describe the entire range of light levels of phytoplankton, Platt et al. [19, 20] proposed another empirical model with a photoinhibition function (model 2 in this study). Superficially, the *P-I* curves fitted by model 2 seem to be perfect as other studies [44, 45], but the value of P_s among the fitted results was notably higher than the value of P_{nmax} in seven phytoplankton strains, whether $\beta > 0$ or $\beta = 0$ (Table 4). However, $P_{nmax} = P_s$ by Eqn. 7, where there was no inhibition at $\beta = 0$, and the fitting curves were similar to model 1 (Fig. 6). Additionally, P_s appeared to fluctuate at $\beta > 0$, which indicates the presence of inhibition among *I. galbana*, *M. aeruginosa*, *M. wesenbergii* and *S. obliquus*. This reveals a clear disagreement with the definition of P_s that characterizes the output of dark reactions of photosynthesis in model 2. Therefore, improvement of model 2 is needed to redefine the biological implication of some fundamental parameters according to the

353 photosynthesis mechanism.

354 Compared with previous models, model 3 is no longer just a mathematical equation
355 describing the dependence of the photosynthetic rate on irradiance intensity. Its
356 foundation is an assumption of “photosynthetic factories” (PSF) on physiological
357 mechanisms proposed by Crill [21]. A PSF that is regarded as a combination of
358 photosystem I (PSI) and PSII conducts one unit of light to generate one unit of
359 photosynthetic product. And Eilers and Peeters assumed that the process of
360 photosynthesis is modeled by changes of the states of PSF from the resting state to the
361 activated and inhibited state [17, 18]. Model 3 yielded a good-fitting curve for the *P-I*
362 data of all strains of phytoplankton in this study, and the returned values for P_{nmax}, I_c, and
363 R_d were close to their measured values, except for I_{sat}, which showed a large deviation (p
364 < 0.05). Meanwhile, Fig. 1c shows that the I_{sat} of curve did not change with the value of
365 β. This may be because there is no assumption of the capture of solar energy, energy
366 transfer process, or electron transport process from PSII to Cytb6f and then to PSI.

367 Although differences between higher plants and phytoplankton are observed in
368 photosynthetic antenna system and photosynthetic components [10, 16], in present study
369 the *P-I* curves of all phytoplankton species fitted by model 4, which be developed for
370 higher plants, were good and the returned values were also close to the measured data.
371 This reveals that *P-I* models for higher plants are applicable for phytoplankton. Acquiring
372 an accurate and optimal parameter for irradiance intensity is essential to achieve high
373 biomass of phytoplankton in production. Irradiance is rapidly attenuated during high-cell
374 density cultivation of phytoplankton [14, 25]. Variation in the pigment composition of
375 light harvesting complexes with irradiance intensity has been observed in most species of
376 phytoplankton [4, 5]. Irradiance intensity also regulates the accumulation of

triacylglycerols and carbohydrates [6, 7]. Note that obtained I_{sat} by model 4 was closer to the measured value than other three models. The differences between the returned values for P_{nmax}, I_c, and R_d by model 4 and their measured values were slightly larger than those by model 3, without significant differences ($p > 0.05$). The fitting curves by model 4 for *P. subcordiformis*, *M. aeruginosa*, *M. wesenbergii*, and *Chlorococcum* sp. exhibited some deviations under low intensity of irradiance, likely because the model targeted higher plants, which showed higher light dependence than phytoplankton.

In meso- and eutrophic water bodies, irradiance or temperature is a key factor affecting changes of phytoplankton community composition, especially for those that become the dominant population between cyanobacteria and green algae [46]. The results of this study explicitly demonstrate that *M. aeruginosa* and *M. wesenbergii* had high intrinsic quantum efficiency (α), while their Chl *a* content per cell was lower than that of both *S. obliquus* and *Chlorococcum* sp., indicating the efficient light harvesting and use for *M. aeruginosa* and *M. wesenbergii*. In addition, almost two times less α than both *S. obliquus* and *Chlorococcum* sp., and the largest P_{nmax} were found in *M. aeruginosa*. However, *M. aeruginosa* is the main contributor of notorious bloom-forming cyanobacteria in global freshwater bodies, such as Dianchi Lake in China [47]. These results reveal the underlying physiological basis of photosynthesis of *Microcystis* with lower "critical light intensity", and provide important insights into the management and control of cyanobacteria in changing lakes and estuarine waters.

I. galbana and *D. salina* are applied world-wide to generate biofuels due to their rich lipids (lipid levels between 23 and 55% by weight of dry biomass), and they are also commonly cultivated with *P. subcordiformis* (lipid levels between 20 and 30% by weight of dry biomass) for aquaculture in China, Japan, Australia, and southeast Asia [14, 48].

To meet nutritional requirements, mixed cultures of two or more species of phytoplankton are often fed to larvae in seed faming of aquatic products [49]. It is critical that the photosynthetic productivity of each strain reach as high as possible during production. The comparison revealed that, although the P_{nmax} lay between *I. galbana* and *P. subcordiformis*, other photosynthetic characteristic parameters showed great differences. The smallest α and highest I_c were found in *I. galbana*, which meant a low efficiency of light capture and use for *I. galbana* because the intrinsic quantum yield represents the numbers of photosynthetic electrons required to assimilate one CO_2 molecule [8]. In contrast, the largest α and lowest I_{sat} and I_c were in *P. subcordiformis*, although it possesses lower Chl *a* content per cell than that of *D. salina*. Consequently, the ranking of light-dependence in descending order was *P. subcordiformis*, *D. salina*, and *I. galbana*. Under co-culture conditions, a gradient of irradiance from low to mid to high can be supplied in one photoperiod.

Conclusions

Our study showed that significant differences were found between the returned values to photosynthetic characteristics by models 1, 2 and 3, some parameters (e.g., I_{sat}) were distinctly different to the measured data. Model 4 for higher plants reproduced the irradiance response trends of photosynthesis well, was applicable for phytoplankton, but more studies are required to investigate its flexibility and reusability. Differences in photosynthetic performance were observed among phytoplankton species. *P. subcordiformis* showed higher light-dependence than *D. salina* and *I. galbana*, while *M. aeruginosa* and *M. wesenbergii* exhibited more efficient light use than *S. obliquus* and *Chlorococcum* sp.. These findings could contribute to a better understanding of structure changes of phytoplankton communities in the aquatic ecosystem, especially in those

425 eutrophic lakes and estuaries.

426

427 **List of abbreviations**

428 Photosystem I (PSI);

429 Photosystem II (PSII);

430 Reactive oxygen species (ROS);

431 Response of photosynthesis to irradiance (*P-I*);

432 Photosynthetic factories (PSF);

433 Chlorophyll *a* (Chl *a*);

434 Irradiance intensity (I, μmol photons m^{-2} s^{-1});

435 Net photosynthetic rate at irradiance I (P_n, μmol O_2 mg^{-1} Cha h^{-1});

436 Maximum net photosynthetic rate (P_{nmax}, μmol O_2 mg^{-1} Cha h^{-1});

437 Saturation irradiance (I_{sat}, μmol photons m^{-2} s^{-1});

438 Light-limited initial slope (α, μmol O_2 mg^{-1} Cha h^{-1} /μmol photons m^{-2} s^{-1});

439 Light compensation point (I_c, μmol photons m^{-2} s^{-1});

440 Dark respiration rate (R_d, μmol O_2 mg^{-1} Cha h^{-1});

441 Adjusted coefficient of determination (R^2);

442 Photosynthetic quantum efficiency (P_n', μmol O_2 μmol photons $^{-1}$);

443 Response of photosynthetic quantum efficiency to irradiance (P_n'-I);

444 Parameter reflecting the maximum, potential, light-saturated, rate of photosynthesis in

445 model 2 (P_s);

446 Photosynthetic pigment molecules (*Chl*);

447 Excited state of photosynthetic pigment molecules (*Chl**).

448

Ethics approval and consent to participate

Not applicable

Consent for publication

All authors consented to the publication of this work.

Availability of data and materials

The datasets supporting the conclusions of this article are included within the article.

Competing interests

The authors declare no competing interests.

Funding

This research was supported by the Natural Science Foundation of China (Grant No. 31960054).

Authors´ contributions

XLY conceived the original study, wrote the paper. XLY and LHL performed the experiment and data analysis. XYW and ZKY conducted the isolation and identification of marine phytoplankton. SBW and ZPY supervised the experiment and editing of paper. All authors read and approved the manuscript.

Acknowledgements

We thanks to the Natural Science Foundation granted by National Natural Science

Foundation of China for financial support in this research. We gratefully acknowledge the anonymous reviewers for their constructive and positive comments. I also would like to express my deepest thanks to my family in Ji'an city, China for their love and support.

Authors´ information

SBW is currently a Professor at Fudan University, China. ZPY is currently a Professor at Jinggangshan University, China. XLY is currently a Ph.D. student at Fudan University, China. LHL is a research assistant at Jinggangshan University, China. ZKY and XYW are two graduate students at Fudan University.

References

1. Novak T, Godrijan J, Pfannkuchen DM, Djakovac T, Medic N, Ivancic I, Mlakar M, Gasparovic B (2019) Global warming and oligotrophication lead to increased lipid production in marine phytoplankton. Science of the Total Environment 668, 171-183.

2. Kwiatkowski L, Aumont O, Bopp L, Ciais P (2018) The impact of variable phytoplankton stoichiometry on projections of primary production, food quality, and carbon uptake in the global ocean. Global Biogeochemical Cycles 32, 516-528.

3. Pachiappan P, Santhanam P, Begum A, Prasath BB (2019) An Introduction to Plankton. In: Santhanam P, Begum A, Pachiappan P (ed) Basic and Applied Microalgae Biology. Berlin, Springer, pp 1-24.

4. Borowitzka M (2019) Commercial-scale production of microalgae for bioproducts. In: La Barre S, Bates SS (ed) Blue Biotechnology -Production and Use of Marine Molecules. New Jersey, Wiley, pp 33-65.

496 5. Ho SH, Ye X, Hasunuma T, Chang JS, Kondo A (2014) Perspectives on engineering
497 strategies for improving biofuel production from microalgae-a critical review.
498 Biotechnology Advances 32, 1448-1459.
499 6. Racault MF, Raitsos DE, Berumen ML, Brewin RJ, Platt T, Sathyendranath S, Hoteit I
500 (2015) Phytoplankton phenology indices in coral reef ecosystems: application to ocean-
501 color observations in the Red Sea. Remote Sensing of Environment 160, 222-234.
502 7. Geider RJ, MacIntyre HL (2001) Physiology and biochemistry of photosynthesis and
503 algal carbon acquisition. In: Williams PJ le B, Thomas DN, Reynolds CS (ed) Microalgae
504 Productivity: Carbon Assimilation in Marine and Freshwater Ecosystems. Oxford,
505 Blackwell Science, pp 44-77.
506 8. Stephenson PG, Moore CM, Terry MJ, Zubkov MV, Bibby TS (2011) Improving
507 photosynthesis for algal biofuels: toward a green revolution. Trends in Biotechnology 29,
508 615-623.
509 9. Ogbonna JC, Tanaka H (2000) Light requirement and photosynthetic cell cultivation–
510 development of processes for efficient light utilization in photobioreactors. Journal of
511 Applied Phycology 12, 207-218.
512 10. Kieselbach T, Cheregi O, Green BR, Funk C (2018) Proteomic analysis of the
513 phycobiliprotein antenna of the cryptophyte alga *Guillardia theta* cultured under different
514 light intensities. Photosynthesis Research 135, 149-163.
515 11. Pathak J, Ahmed H, Singh PR, Singh SP, Häder D-P, Sinha RP (2019) Mechanisms of
516 Photoprotection in Cyanobacteria. In: Mishra AK, Tiwari DN, Rai AN (ed) Cyanobacteria.

517 London, Academic press, pp 145-171.
518 12. Huete-Ortega M, Okurowska K, Kapoore RV, Johnson MP, Gilmour DJ, Vaidyanathan
519 S (2018) Effect of ammonium and high light intensity on the accumulation of lipids in
520 *Nannochloropsis oceanica* (CCAP 849/10) and *Phaeodactylum tricornutum* (CCAP
521 1055/1). Biotechnology for biofuels 11, 60.
522 13. Wang HT, Meng YY, Cao XP, Ai JN, Zhou JN, Xue S, Wang WL (2015) Coordinated
523 response of photosynthesis, carbon assimilation, and triacylglycerol accumulation to
524 nitrogen starvation in the marine microalgae *Isochrysis* zhangjiangensis (Haptophyta).
525 Bioresource Technology 177, 282-288.
526 14. Abu-Ghosh S, Dubinsky Z, Banet G, Iluz D (2018) Optimizing photon dose and
527 frequency to enhance lipid productivity of thermophilic algae for biofuel production.
528 Bioresource Technology 260, 374-379.
529 15. Burson A, Stomp M, Greenwell E, Grosse J, Huisman J (2018) Competition for
530 nutrients and light: testing advances in resource competition with a natural phytoplankton
531 community. Ecology 99, 1108-1118.
532 16. Darvehei P, Bahri PA, Moheimani NR (2018) Model development for the growth of
533 microalgae: A review. Renewable and Sustainable Energy Reviews 97, 233-258.
534 17. Eilers PHC, Peeters JCH (1988) A model for the relationship between light intensity
535 and the rate of photosynthesis in phytoplankton. Ecological Modelling 42, 199-215.
536 18. Platt T, Harrison WG, Irwin B, Horne EP, Gallegos CL (1982) Photosynthesis and
537 photoadaptation of marine phytoplankton in the arctic. Deep Sea Research Part A

538 Oceanographic Research Papers 29, 1159-1170.
539 19. Platt T, Gallegos C, Harrison WG (1980) Photoinhibition of photosynthesis in natural
540 assemblages of marine phytoplankton. Journal of Marine Research 38, 687-701.
541 20. Crill PA (1977) The photosynthesis-light curve: A simple analog model. Journal of
542 Theoretical Biology 64, 503-516.
543 21. Platt T, Jassby AD (1976) The relationship between photosynthesis and light for
544 natural assemblages of coastal marine phytoplankton. J Phycol 12, 421-430.
545 22. Webb WL, Newton M, Starr D (1974) Carbon dioxide exchange of *Alnus rubra*. A
546 mathematical model. Oecologia 17, 281-291.
547 23. Jayaraman SK, Rhinehart RR (2015) Modeling and optimization of algae growth.
548 Industrial & Engineering Chemistry Research 54, 8063-8071.
549 24. Bechet Q, Chambonniere P, Shilton A, Guizard G, Guieysse B (2015) Algal
550 productivity modeling: a step toward accurate assessments of full-scale algal cultivation.
551 Biotechnology and Bioengineering 112, 987-996.
552 25. Garcia-Camacho F, Sanchez-Miron A, Molina-Grima E, Camacho-Rubio F,
553 Merchuck JC (2012) A mechanistic model of photosynthesis in microalgae including
554 photoacclimation dynamics. Journal of Theoretical Biology 304, 1-15.
555 26. Bernard O, Remond B (2012) Validation of a simple model accounting for light and
556 temperature effect on microalgal growth. Bioresource Technology 123, 520-527.
557 27. Rubio FC, Camacho FG, Sevilla JM, Chisti Y, Grima EM (2003) A mechanistic model
558 of photosynthesis in microalgae. Biotechnology and Bioengineering 81, 459-473.

559 28. Han BP (2001) Photosynthesis–irradiance response at physiological level: a
560 mechanistic model. Journal of Theoretical Biology 213, 121-127.
561 29. Bannister TT (1979) Quantitative description of steady state, nutrient-saturated algal
562 growth, including adaptation. Limnology and Oceanography 24, 76-96.
563 30. Chen B, Zou D, Ma Z, Yu P, Wu M (2019) Effects of light intensity on the
564 photosynthetic responses of *Sargassum fusiforme* seedlings to future CO_2 rising.
565 Aquaculture Research 50, 116-125.
566 31. Hill EA, Chrisler WB, Beliaev AS, Bernstein HC (2017) A flexible microbial co-
567 culture platform for simultaneous utilization of methane and carbon dioxide from gas
568 feedstocks. Bioresource Technology 228, 250-256.
569 32. Kim M, Brodersen KE, Szabó M, Larkum AWD, Raven JA, Ralph PJ, Pernice M
570 (2018) Low oxygen affects photophysiology and the level of expression of two-carbon
571 metabolism genes in the seagrass *Zostera muelleri*. Photosynthesis Research 136, 147-
572 160.
573 33. Ma Z, Fang T, Thring RW, Li Y, Yu H, Zhou Q, Zhao M (2015) Toxic and non-toxic
574 strains of *Microcystis aeruginosa* induce temperature dependent allelopathy toward
575 growth and photosynthesis of Chlorella vulgaris. Harmful Algae 48, 21-29.
576 34. Park J, Dinh TB (2019) Contrasting effects of monochromatic LED lighting on growth,
577 pigments and photosynthesis in the commercially important cyanobacterium Arthrospira
578 maxima. Bioresource Technology 291, 121846.
579 35. Ye ZP, Suggett DJ, Robakowski P, Kang HJ (2013) A mechanistic model for the

580 photosynthesis-light response based on the photosynthetic electron transport of
581 photosystem II in C3 and C4 species. New Phytologist 199, 110-120.
582 36. Li X, Cai J, Liu F, Dai T, Cao W, Jiang D (2014) Exogenous abscisic acid application
583 during grain filling in winter wheat improves cold tolerance of offspring's seedlings.
584 Journal of Agronomy Crop Science 200, 467-478.
585 37. Wu A, Song Y, Van Oosterom EJ, Hammer GL (2016) Connecting biochemical
586 photosynthesis models with crop models to support crop improvement. Frontiers in Pant
587 Science 7, 1518.
588 38. Jeffrey SW, Humphrey GFJBUPDP (1975) New spectrophotometric equations for
589 determining chlorophylls *a*, *b*, *c*1 and *c*2 in higher plants, algae and natural phytoplankton.
590 Biochemie Und Physiologie Der Pflanzen 167, 191-194.
591 39. Bouman HA, Platt T, Doblin M, Figueiras FG, Sathyendranath S (2017)
592 Photosynthesis-irradiance parameters of marine phytoplankton: synthesis of a global data
593 set. Earth System Science Data 10, 1-32.
594 40. Kok B (1948) A critical consideration of the quantum yield of *Chlorella*
595 photosynthesis. Enzymologia 13, 1-56.
596 41. Ye ZP (2012) Nonlinear optical absorption of photosynthetic pigment molecules in
597 leaves. Photosynthesis Research 112, 31-37.
598 42. Ooms MD, Dinh CT, Sargent EH, Sinton D (2016) Photon management for
599 augmented photosynthesis. Nature Communications 7, 12699.
600 43. Baly ECC (1935) The kinetics of photosynthesis. Proceedings of the Royal Society

601 of London 149, 596-596.
602 44. Vu MTT, Douëtte C, Rayner TA, Thoisen C, Nielsen SrL, Hansen BW (2016)
603 Optimization of photosynthesis, growth, and biochemical composition of the microalga
604 *Rhodomonas salina*—an established diet for live feed copepods in aquaculture. Journal
605 of Applied Phycology 28, 1485-1500.
606 45. Stawiarski B, Buitenhuis ET, Fallens M (2018) The physiological response of seven
607 strains of picophytoplankton to light, and its representation in a dynamic photosynthesis
608 model. Limnology Oceanography 63, 367-380.
609 46. Chisti Y (2007) Biodiesel from microalgae. Biotechnology Advances 25, 294-306.
610 47. Ehteshami F, Romano N, Ramezani Fard E, Hoseinzadeh Sahafi H (2017) Effect of
611 different dietary microalgae combinations on growth and survival of black‐lip pearl
612 oyster (*Pinctada margaritifera*) larvae and the feasibility of replacing microalgae with a
613 dietary lipid emulsion. Aquaculture Nutrition 23, 671-680.
614 48. Qian Y, Liu Z, Chen Y, Zhu D, Na L (2018) Modelling the impact of hydrodynamic
615 turbulence on the competition between *Microcystis* and *Chlorella* for light. Ecological
616 Modelling 370, 50-58.
617 49. Yang X, Liu L, Wang S (2019) A strategy of high-efficient nitrogen removal by an
618 ammonia-oxidizing bacterium consortium. Bioresource Technology 275, 216-224.
619
620
621
622

623

624 **Table and Figure captions**

625 **Table 1** The Chlorophyll *a* content and cell number profiles of seven phytoplankton
626 cultures.

627 **Table 2** Comparison of the results fitted by Models 1, 2, 3 and 4 with measured data in
628 marine phytoplankton.

629 **Table 3** Comparison of the results fitted by Models 1, 2, 3 and 4 with measured data in
630 freshwater phytoplankton.

631 **Table 4** Comparison of P_s and P_{nmax} (μmol $O_2 \cdot mg^{-1}$ Cha$\cdot h^{-1}$) calculated by model 2 with
632 measured values

633 **Fig. 1** Model 2, Model 3 and Model 4 responses of the net photosynthetic rate (P_n) versus
634 irradiance intensity (I) determined for the different values of the fundamental parameters,
635 respectively. (a) and (b) were obtained by Model 2, (c) and (d) were obtained by Model
636 3, and (e) and (f) were obtained by Model 4.

637 **Fig. 2** The *P-I* curves (A) and *P′-I* curves (B) of *Isochrysis galbana*, *Dunaliella salina*
638 and *Platymonus subcordiformis*.

639 **Fig. 3** The *P-I* curves (A) and *P′-I* curves (B) of *Microcystis aeruginosa*, *Microcystis*
640 *wesenbergii*, *Scenedesmus obliquus* and *Chlorococcum* sp..

641 **Fig. 4** Schematic representation of the mechanism of photosynthesis consisting of
642 biophysical and biochemical processes.

643 **Fig. 5** The *P-I* curves produced by the model 2 at $\beta = 0$ and $\beta > 0$.

644

645

646

647

648 **Table 1** The Chlorophyll *a* content and cell number profile of seven phytoplankton cultures.

Strains	Chl *a* (mg L^{-1})	Cell density (10^4 cells mL^{-1})	Cell size (μm)
Isochrysis galbana	1.647±0.015	641.00±5.95	5.8±0.4
Dunaliella salina	2.778±0.077	103.00±7.00	9.8±0.2
Platymonus subcordiformis	2.297±0.027	100.33±3.38	10.0±0.1
Microcystis aeruginosa FACHB-905	1.320±0.005	669.67±12.35	4.3±0.4
Microcystis wesenbergii FACHB-1112	1.739±0.012	723.33±5.18	5.1±0.2
Scenedesmus obliquus FACHB-116	1.318±0.027	145.33±6.64	8.1±0.5
Chlorococcum sp. FACHB-1556	4.158±0.077	908.67±14.08	6.0±1.2

649

650 **Table 2** Comparison of results fitted by Model 1, 2, 3 and 4 with measured data in marine
651 phytoplankton.

Models	Photosynthetic parameters					
	α (μmol O_2 mg^{-1} Chl *a* h^{-1} /μmol photons m^{-2} s^{-1})	P_{nmax} (μmol O_2 mg^{-1} Chl *a* h^{-1})	I_{sat} (μmol photons m^{-2} s^{-1})	I_c (μmol photons m^{-2} s^{-1})	R_n (μmol O_2 mg^{-1} Chl *a* h^{-1})	R^2
Isochrysis galbana						
Model 1	0.411±0.032[a]	119.51±4.72[a]	229.90±13.60[b]	63.12±2.33[a]	25.97±2.54[a]	0.981±0.007[a]
Model 2	0.468±0.037[a]	97.45±3.02[b]	709.60±26.89[a]	56.71±2.41[a]	26.59±2.60[a]	0.986±0.007[a]
Model 3	0.373±0.020[a]	97.55±3.37[b]	699.26±32.19[a]	65.51±3.48[a]	23.98±1.95[a]	0.989±0.007[a]
Model 4	0.482±0.037[a]	98.33±3.20[b]	766.17±24.38[a]	61.06±2.82[a]	26.63±2.44[a]	0.986±0.008[a]
Measured		≈ 94.14	≈ 800	≈ 62	≈ 24.29	
Dunaliella salina						
Model 1	0.874±0.023[c]	123.09±5.88[a]	116.90±23.87[c]	23.87±1.66[a]	20.92±1.97[a]	0.944±0.016[b]
Model 2	1.006±0.033[b]	113.73±6.24[a]	453.39±6.87[b]	21.27±1.75[a]	21.39±1.81[a]	0.990±0.001[a]
Model 3	0.918±0.058[bc]	114.45±6.24[a]	444.33±6.04[b]	23.09±2.29[a]	19.89±1.14[a]	0.989±0.007[a]
Model 4	1.202±0.037[a]	113.31±5.87[a]	510.24±2.92[a]	21.67±1.93[a]	23.30±1.93[a]	0.983±0.002[a]
Measured		≈119.24	≈500	≈23	≈20.25	
Platymonus subcordiformis						
Model 1	1.975±0.055[d]	107.96±5.58[a]	41.25±1.62[d]	13.40±2.21[a]	26.32±3.93[a]	0.883±0.010[c]
Model 2	2.479±0.023[c]	94.64±6.65[a]	212.36±7.80[c]	11.05±1.65[a]	27.45±4.30[a]	0.975±0.009[a]
Model 3	2.834±0.056[b]	95.59±6.63[a]	251.97±9.73[b]	10.82±1.87[a]	26.13±4.26[a]	0.958±0.013[ab]
Model 4	3.640±0.031[a]	92.20±6.56[a]	299.55±10.72[a]	9.68±1.71[a]	28.36±4.21[a]	0.934±0.013[b]
Measured		≈100.13	≈150	≈14	≈24.49	

652

653

Table 3 Comparison of results fitted by Model 1, 2, 3 and 4 with measured data in freshwater phytoplankton.

Models	Photosynthetic parameters					
	α (μmol O_2 mg^{-1} Chl *a* h^{-1} /μmol photons m^{-2} s^{-1})	P_{nmax} (μmol O_2 mg^{-1} Chl *a* h^{-1})	I_{sat} (μmol photons m^{-2} s^{-1})	I_c (μmol photons m^{-2} s^{-1})	R_d (μmol O_2 mg^{-1} Chl *a* h^{-1})	R^2
Microcystis aeruginosa						
Model 1	2.404±0.103^{b}	260.46±10.72^{a}	97.83±2.42^{d}	10.57±1.12^{a}	25.63±3.86^{a}	0.721±0.047^{b}
Model 2	2.416±0.074^{b}	290.74±15.09^{a}	380.17±4.89^{b}	9.47±1.05^{a}	22.92±2.75^{a}	0.973±0.010^{a}
Model 3	1.770±0.026^{c}	296.37±14.89^{a}	340.82±4.49^{c}	10.26±2.54^{a}	18.23±4.61^{a}	0.969±0.015^{a}
Model 4	2.967±0.067^{a}	283.55±14.53^{a}	415.25±2.33^{a}	9.53±1.05^{a}	26.86±2.75^{a}	0.964±0.007^{a}
Measured		≈ 290.83	≈ 400	≈ 10	≈ 18.27	
Microcystis wesenbergii						
Model 1	1.879±0.039^{b}	184.72±2.57^{c}	82.57±2.56^{d}	15.85±1.68^{a}	29.73±2.91^{ab}	0.758±0.031^{b}
Model 2	1.920±0.030^{b}	195.32±1.50^{ab}	352.20±7.29^{b}	14.70±1.87^{a}	28.15±2.44^{ab}	0.974±0.006^{a}
Model 3	1.309±0.074^{c}	201.37±2.94^{a}	322.50±6.96^{c}	15.50±2.37^{a}	20.46±3.90^{b}	0.978±0.007^{a}
Model 4	2.474±0.071^{a}	188.62±2.31^{bc}	389.62±9.62^{a}	14.81±1.47^{a}	33.19±2.31^{a}	0.954±0.011^{a}
Measured		≈ 201.29	≈ 400	≈ 15	≈ 23.73	
Scenedesmus obliquus						
Model 1	1.499±0.019^{c}	265.88±5.70^{a}	159.64±1.84^{d}	17.82±3.32^{a}	26.61±4.67^{a}	0.912±0.006^{b}
Model 2	1.581±0.010^{b}	268.80±5.21^{a}	527.39±8.93^{b}	15.24±3.18^{a}	24.05±4.91^{a}	0.989±0.002^{a}
Model 3	1.268±0.030^{d}	268.70±5.25^{a}	481.60±8.51^{c}	15.34±3.74^{a}	19.25±4.59^{a}	0.989±0.001^{a}
Model 4	1.751±0.021^{a}	268.11±4.98^{a}	561.94±8.40^{a}	15.82±3.15^{a}	26.29±4.79^{a}	0.987±0.002^{a}
Measured		≈ 267.37	≈ 400	≈ 15	≈ 19.91	
Chlorococcum sp.						
Model 1	0.979±0.007^{c}	83.86±4.98^{a}	68.66±4.47^{c}	17.00±1.80^{a}	16.66±1.82^{a}	0.935±0.009^{c}
Model 2	1.190±0.020^{b}	75.25±3.79^{a}	311.04±17.27^{b}	14.59±1.52^{a}	17.43±2.09^{a}	0.984±0.001^{a}
Model 3	1.247±0.022^{b}	76.15±3.89^{a}	339.85±15.19^{b}	15.02±1.76^{a}	16.82±2.09^{a}	0.979±0.002^{ab}
Model 4	1.572±0.024^{a}	74.59±4.23^{a}	396.06±15.93^{a}	13.87±1.59^{a}	18.64±2.18^{a}	0.964±0.001^{b}
Measured		≈76.06	≈ 400	≈ 15	≈ 15.03	

663

664

665 **Table 4** Comparison of P_s, P_{nmax} (μmol O_2 mg^{-1} Chl *a* h^{-1}) calculated by model 2 with measured value

Parameter	*Isochrysis galbana*	*Dunaliella salina*	*Platymonus subcordiformis*	*Microcystis aeruginosa*	*Microcystis wesenbergii*	*Scenedesmus obliquus*	*Chlorococcum* sp.
P_s ($\beta = 0$)	135.44±6.59	144.28±10.86	133.39±6.73	328.48±18.27	235.77±3.70	311.42±7.37	96.21±5.71
P_s ($\beta > 0$)	14188.6±13735.8	196.08±31.06	135.23±7.45	1163.4±615.5	415.53±29.50	943.8±282.4	107.02±5.53
P_{nmax}	97.45±3.02	113.73±6.24	94.64±6.65	290.74±15.09	195.32±1.50	268.80±5.21	75.25±3.79
Observations	≈94	≈119	≈100	≈290	≈200	≈267	≈75

666

667

668

669

670

671

672

673

674

675

676

677

678

679

680

681

682

683

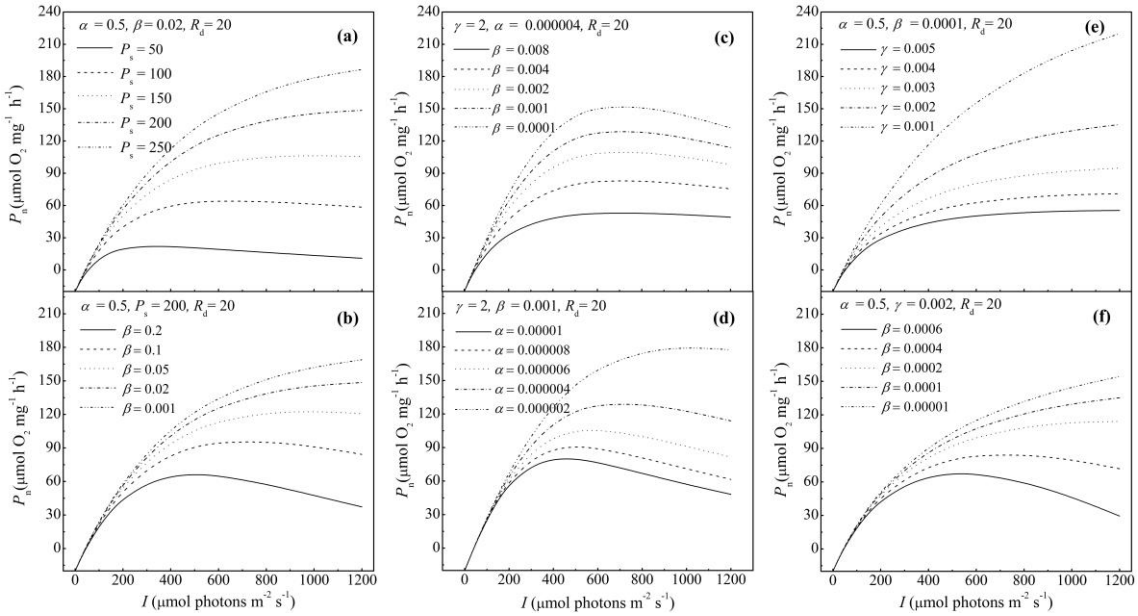

Fig. 1 Model 2, Model 3 and Model 4 responses of the net photosynthetic rate (P_n) versus irradiance intensity (I) determined for different values of the fundamental parameters, respectively. (a) and (b) were obtained by Model 2, (c) and (d) were obtained by Model 3, (e) and (f) were obtained by Model 4.

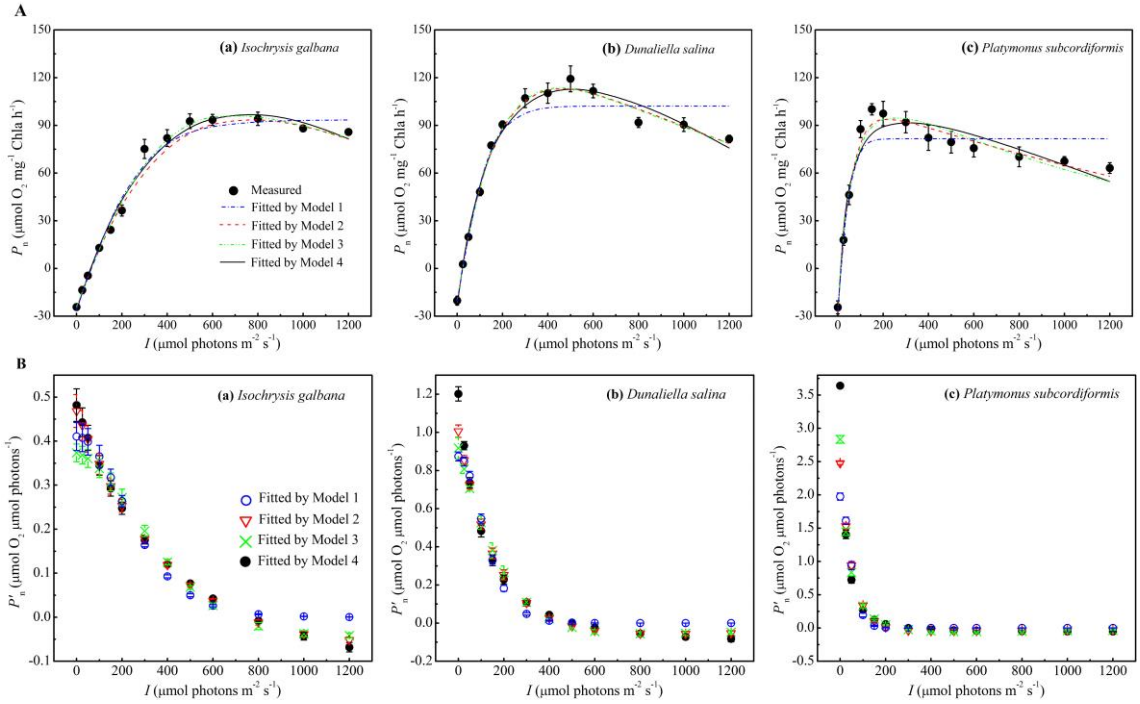

Fig. 2 The *P*-*I* curves (A) and *P*′-*I* curves (B) in *Isochrysis galbana*, *Dunaliella salina* and *Platymonus*

693 *subcordiformis*.

694

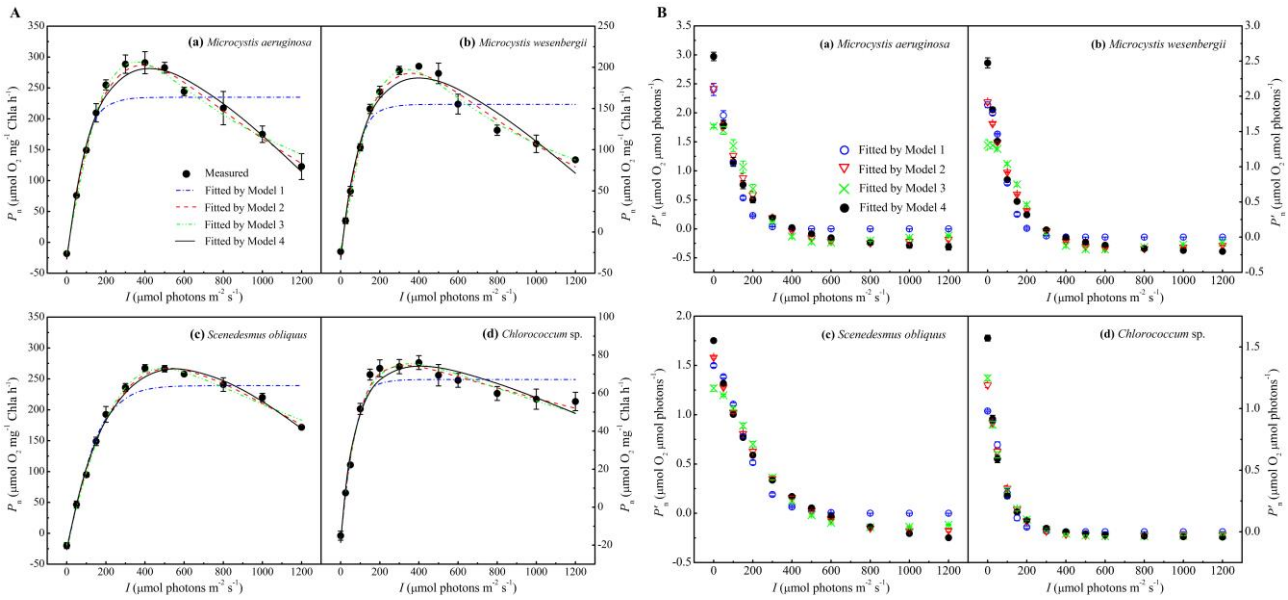

695

696 **Fig. 3** The *P-I* curves (A) and *P′-I* curves (B) in *Microcystis aeruginosa*, *Microcystis wesenbergii*,

697 *Scenedesmus obliquus* and *Chlorococcum* sp..

698

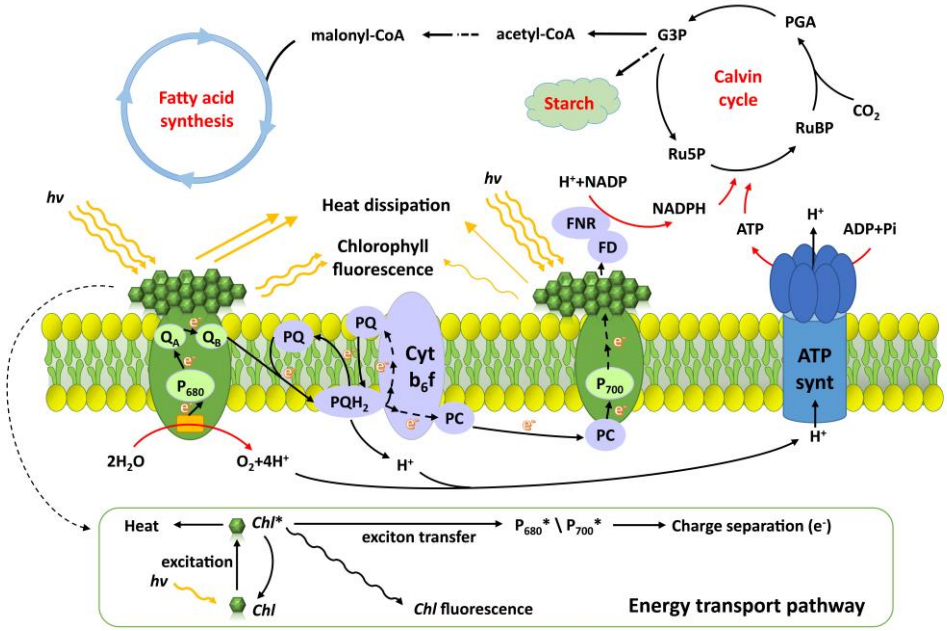

699

700 **Fig. 4** Schematic representation of mechanism of photosynthesis consisted of biophysical and

701 biochemical processes.

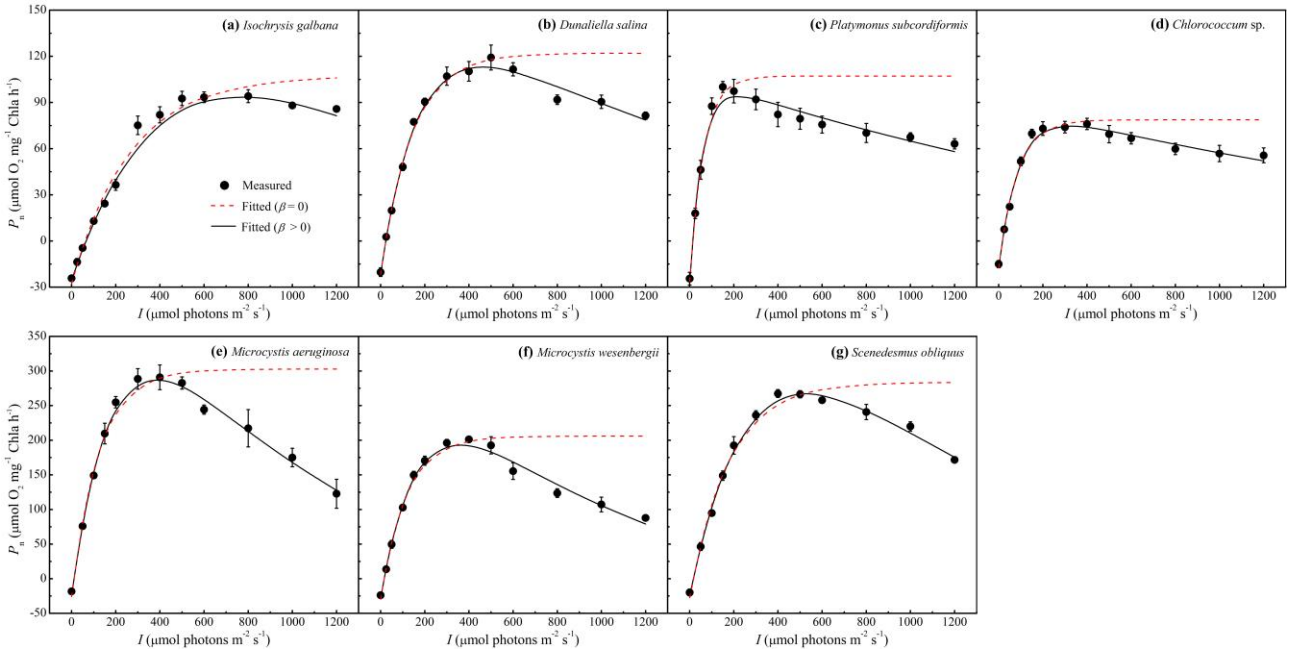

Fig. 5 The *P-I* curves produced by the model 2 at $\beta = 0$ and $\beta > 0$.